

Towards quantum attractors: Sampling asymptotic states of modulated open systems with quantum trajectories

V. Volokitin^a, A. Liniov^b, I. Meyerov^a, M. Hartmann^d, M. Ivanchenko^c, P. Hänggi^{d,c}, S. Denisov^{d,c,*}

^aMathematical Software and Supercomputing Technologies Department, Lobachevsky State University of Nizhny Novgorod, Russia

^bDepartment of Software Engineering, Lobachevsky State University of Nizhny Novgorod, Russia

^cDepartment of Applied Mathematics, Lobachevsky State University of Nizhny Novgorod, Russia

^dInstitut für Physik, Universität Augsburg, Universitätsstraße 1, D-86135 Augsburg, Germany

Abstract

Quantum systems out of equilibrium are now a subject of intensive research both in theoretical and experimental physics. In this paper we study periodically modulated quantum systems which are in contact with a stationary environment. Within the framework of Lindblad quantum master equation, the asymptotic states of such systems are described by time-periodic density operators. Resolution of these operators is a non-trivial computational task. Approaches based on spectral and iterative methods are restricted to systems with the dimension of the hosting Hilbert space $\dim\mathcal{H} = N \lesssim 300$, while the direct long-time integration of the master equation becomes problematic for $N \gtrsim 400$. To overcome these limitations we use the quantum trajectory method which unravels the deterministic master equation for the density operator into a set of stochastic processes for wave functions. This method avoids calculations of the kernel of the Floquet superoperator; instead the asymptotic density matrix is calculated by performing a statistical sampling preceded by a long transient propagation. We present a high-accuracy realization of this idea based on exponential propagators combined with a time-stepping technique. Employing a scalable model of interacting bosons hopping over a dimer, we test the performance of the algorithm on a supercomputer. We demonstrate that the algorithm allows to resolve non-equilibrium asymptotic states of model systems with $\dim\mathcal{H} \simeq 2000$ on a small computer cluster thus reaching the scale on which numerical studies of isolated periodically-modulated systems are currently performed.

Keywords: open quantum systems, Lindblad equation, periodic modulations, quantum trajectories

1. Introduction

Any *in vivo* quantum system is in a contact with its environment. Although typically weak, this interaction becomes relevant when studying the evolution of a system over long time scales. In particular, the asymptotic state of such an *open* system depends both on the unitary action induced by the system Hamiltonian, and the action of the environment, conventionally called ‘dissipation’. A recent idea of “engineering by dissipation” [1, 2, 3, 4], the creation of designated pure and highly entangled states of many-body quantum systems by using specially designed dissipative operators, has promoted dissipation to the same level of importance as the underlying unitary dynamics.

The use of time-periodic modulations constitutes another channel to impact states of a quantum system. In the coherent limit, when the system is isolated from the environment, modulations imply an explicit time-periodicity of the system Hamiltonian, $H(t + T) = H(t)$. The dynamics of the system are determined by the basis of time-periodic *Floquet eigenstates* [5, 6, 7, 8]. The properties of the Floquet states de-

pend on various modulation parameters. Modulations being resonant with intrinsic system frequencies can create a set of non-equilibrium eigenstates with properties drastically different from those with time-independent Hamiltonians. Modulations enrich the physics occurring in fields such as quantum optics, optomechanics, solid state and ultra-cold atom physics [7, 9, 10, 11, 12] and disclose a spectrum of new phenomena [13, 14, 15, 16].

What are the possible prospects of a synergy between environment-induced decoherence and periodic modulations when both impact a N -state system? Indeed, this question can be rephrased more precisely, depending on the context of the problem. We are confident though that the answer even to this general question will be appreciated by several communities working on many-body localization (MBL) [17, 18, 19, 20, 21, 22], Floquet topological insulators [14], and dissipative engineering [1, 2, 3].

There exist several approaches to model the evolution of an open quantum systems [23]; the most popular, especially in the context of quantum optics [24], is the quantum master equation

*Corresponding author at: Institut für Physik, Universität Augsburg, Universitätsstraße 1, D-86135 Augsburg, Germany

Email address: sergey.denisov@physik.uni-augsburg.de (S. Denisov)

with its generator \mathcal{L} in Lindblad form [25, 26] (we set $\hbar = 1$):

$$\begin{aligned}\dot{\varrho} &= \mathcal{L}(\varrho) = -i[H(t), \varrho] + \sum_{k=1}^K \gamma_k(t) \cdot \mathcal{D}_k(\varrho), \\ \mathcal{D}_k(\varrho) &= V_k \varrho V_k^\dagger - \frac{1}{2} \{V_k^\dagger V_k, \varrho\}.\end{aligned}\quad (1)$$

Here, ϱ denotes the system density matrix, while the set of quantum jump operators, V_k , $k = 1, \dots, K$, capture the action of the environment on the system. The jump operators act via K ‘channels’ with time-dependent rates $\gamma_k(t)$. Finally, $[\cdot, \cdot]$ and $\{\cdot, \cdot\}$ denote the commutator and the anti-commutator, respectively.

As an object of mathematical physics, Eq. (1) has a specific structure and possesses a variety of important properties [26]. In the case of a time-independent, stationary Hamiltonian $H(t) \equiv H$, the generator \mathcal{L} induces a continuous set of completely positive quantum maps $\mathcal{P}_t = e^{\mathcal{L}t}$ [27]. Under some conditions (‘quantum ergodicity’), the system evolves from an initial state ϱ^{init} to a unique and time-independent asymptotic state ϱ_{eq} , $\lim_{t \rightarrow \infty} \mathcal{P}_t \varrho^{\text{init}} = \varrho_{\text{eq}}$ [28, 26, 29]. When time-periodic modulations are present, Eq. (1) preserves the complete positivity of the evolution if all coupling rates are non-negative at any instance of time, $\gamma_k(t) \geq 0$, $\forall t$ [30]. Under some suitable, experimentally relevant assumptions, a set-up ‘‘time-dependent Hamiltonian and time-independent dissipation’’ provides a valid approximation [26].

Here, we address the particular case of quench-like, time-periodic dependence of the Hamiltonian, $H(t) = H(t+T)$, corresponding to periodic switches between several constant Hamiltonians [16]. A popular choice is the set-up composed of two Hamiltonians,

$$H(t) = \begin{cases} H_1, & \text{for } 0 \leq t \bmod T < \tau \\ H_2, & \text{for } \tau \leq t \bmod T < T \end{cases}, \quad (2)$$

where $\tau = t \bmod T$, $\tau \in [0, T]$. This minimal form has recently been used to investigate the connection between integrability and thermalization [19, 31, 32] or, alike, for disorder-induced localization [18] in *isolated* periodically modulated many-body systems.

From a mathematical point of view, Eqs. (1,2) define a linear equation with a time-periodic generator $\mathcal{L}(t)$. Therefore, Floquet theory applies and asymptotic solutions of the equation are all time-periodic with temporal period T [7, 33]. $\mathcal{L}(t)$ is a dissipative operator and, in the absence of relevant symmetries [29], the system evolution in the asymptotic limit $t \rightarrow \infty$ is determined by a unique ‘quantum attractor’, i.e., by an asymptotic, time-periodic density operator, $\varrho^{\text{att}}(\tau + nT) = \varrho^{\text{att}}(\tau)$, $\tau \in [0, T]$ and $n \in \mathbb{Z}^+$. The challenge here consists in explicit numerical evaluation of the matrix form of this operator.

To use spectral methods (complete/partial diagonalization and different kinds of iterative algorithms [34]) to calculate ϱ_{att} as eigen-element of a superoperator would mean to deal with N^2 scaling of computationally expensive operations. In the case of periodically modulated systems it restricts the use of spectral

methods to $N \lesssim 300$ ¹. A direct propagation of Eq. (1) for a time span long enough for $\varrho(t)$ to approach the attractor is not feasible for $N \gtrsim 400$ for two reasons: First, direct propagation requires to numerically propagate $N^2 > 200\,000$ complex differential equations with time-dependent coefficients, and second, accuracy might become a problem for large times. Although the accuracy may be improved by implementing high-order integration schemes [35] or Faber and Newton polynomial integrators [36], this approach is hardly parallelizable².

Systems with $N_{\text{max}} = 400$ states may still be too small, for example, to explore MBL effects in open periodically-modulated systems. Is it possible to go beyond this limit? And if so how far? We attempt to answer these questions by unraveling of the quantum master equation (1) into a set of stochastic realizations, called ‘‘quantum trajectories’’ [38, 39, 40, 41]. This method allows us to transform the problem of the numerical solution of Eqs. (1,2) into a task of statistical sampling over quantum trajectories which form vectors of the size N . The price to pay for the reduction from N^2 to N is that we now have to sample over many realizations. This problem is very well suited for parallelization [42] and we can definitely benefit from the use of a computation cluster. If the number of realizations M_T becomes large, the sampling of the density operator $\varrho(t)$ with initial condition $\varrho^{\text{init}} = |\psi^{\text{init}}\rangle\langle\psi^{\text{init}}|$ converges to the solution of Eq. (1) [38, 39]. This method is popular in the field of quantum optics where it adequately describes the physics of experiments [24].

An important issue is the time t_p when the trajectories are sampled. To guarantee that the asymptotic regime is reached, this time should exceed the longest relaxation timescale of the system. Practically, this means that the sampling at time $t_p = ST$, $S \gg 1$, does converge to a density operator $\varrho(t_p)$ close to $\varrho^{\text{att}}(0)$. In order to minimize propagation errors, we devise an integration scheme based on a set of exponential propagators. For quench-like periodic modulations this implies a finite number of propagators which can be pre-calculated and stored locally on each cluster node.

We address generic systems of the type specified by Eqs. (1,2), with no conditions imposed on operators $H(t)$ and V_k (for example, they need not be local [37]) and with no *a priori* knowledge of the attractor state. For example, the asymptotic state may be strongly entangled [1] and with the purity arbitrary close to 1. For a scalable model, a periodically rocked and dissipatively coupled dimer with $N - 1$ interacting bosons, we find that the statistical variance of the sampling does not grow infinitely with t_p but saturates to a limit-cycle evolution. Therefore, the number of trajectories $M_T(\epsilon)$ needed to estimate elements of ϱ^{att} with accuracy ϵ (defined with some matrix norm)

¹Even if the Hamiltonians H_1, H_2 and the corresponding Lindblad operators $\mathcal{L}_1, \mathcal{L}_2$ are sparse, the Floquet map $\mathcal{P}(T) = e^{\mathcal{L}_2(T-\tau)} e^{\mathcal{L}_1\tau}$ is a dense matrix. Therefore, the numerical evaluation cannot benefit from sparse-matrix methods.

²There is a sophisticated way to propagate Eq. (1) by using the so-called time evolving block decimation (TEBD) technique [37]. The numerical effort scales as $\log N$. However, this algorithm can only be used for lattice systems, i.e., systems that can be partitioned into $\sim \log(N)$ ‘pieces’ coupled by next-neighbor interactions, both unitary and dissipative. In this case it gives a correct answer when the asymptotic state is characterized by a low entanglement.

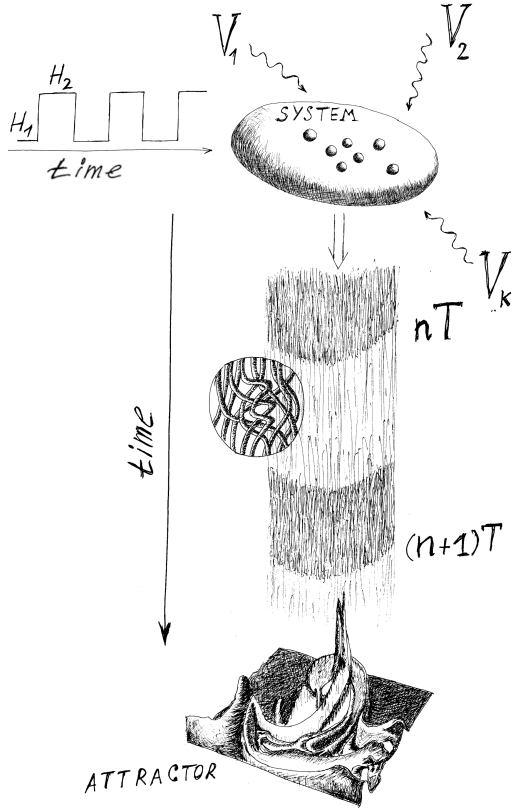


Figure 1: Resolving a quantum attractor with quantum trajectories. To calculate the density matrix $\varrho(t_p)$ of the asymptotic state of an open system, periodically modulated in a quench-like manner, Eq. (2), every trajectory is propagated up to time t_p and then used for the stroboscopic sampling of the matrix elements.

remains finite. Assuming that the propagation can be performed for an arbitrary large time t_p with required accuracy, we are left with the problem of sampling over a sufficiently large number of trajectories. On top, in the asymptotic limit, sampling of $\varrho^{\text{att}}(0)$ can be performed over individual trajectories stroboscopically, after each period T . This increases the efficiency of sampling via the multiple use of the same trajectory, without having to initiate a new trajectory and then propagating it to time t_p . Our results confirm that by implementing this approach (sketched on Fig. 1) on a cluster, it is possible to resolve attractors of periodically modulated open systems with several thousand quantum states, thus increasing N_{max} by an order of magnitude.

The present work is organized as follows: In Section 2 we outline the method of quantum trajectories and describe the algorithm to propagate them. Relevant statistical aspects of the sampling are briefly discussed in Section 3. In Section 4 we introduce a scalable model system. Section 5 is devoted to the implementation of the algorithm on a cluster together with an analysis of its performance and scalability. Section 6 reports numerical results obtained for the model system. Our findings are summarized together with an outline of further perspectives in Section 7.

2. Quantum trajectory as an event-driven process

To sample the solution of Eq. (1) at some time t_p by using the quantum trajectory method (also known under the labels of ‘quantum jump method’ [24, 40] and ‘Monte Carlo wave function method’ [39]) we first have to calculate the effective non-Hermitian Hamiltonian

$$\tilde{H}(t) = H(t) - \frac{i}{2} \sum_{k=1}^K V_k^\dagger V_k, \quad (3)$$

and then proceed along the following set of instructions [38]:

1. initiate the trajectory in a pure state $|\psi^{\text{init}}\rangle$;
2. draw a random number η uniformly distributed on the unit interval;
3. propagate the state $|\psi(t)\rangle$ in time using the effective Hamiltonian $\tilde{H}(t)$;
4. the squared norm $\|\psi(t)\|^2$ decays monotonically; when $\eta = \|\psi(t)\|^2$, stop the propagation and normalize the state vector, $|\psi(t)\rangle \rightarrow |\psi(t)\rangle / \|\psi(t)\|$;
5. perform a quantum jump: select the jump operator D_k with probability $p_k = \gamma_k \|\psi(t)\|^2 / \sum_{k=1}^K \gamma_k \|\psi(t)\|^2$ and apply the transformation $|\psi(t)\rangle \rightarrow D_k |\psi(t)\rangle / \|D_k |\psi(t)\rangle\|$;
6. repeat steps 2 – 5 until the desired time t_p is reached.

The density matrix can then be sampled out of M_r realizations as $\varrho(t_p; M_r) = \frac{1}{M_r} \sum_{j=1}^{M_r} |\psi_j(t_p)\rangle \langle \psi_j(t_p)|$. Formally, in the limit $M_r \rightarrow \infty$, it converges to the solution of Eq. (1) at the time t_p and initial density matrix $\varrho^{\text{init}} = |\psi^{\text{init}}\rangle \langle \psi^{\text{init}}|$ [23, 38]. The density matrix can also be sampled at any other prior instance of time $t \in [0, t_p]$. This will not affect the propagation of the trajectory and only demands normalization of the state vector $|\psi(t)\rangle$ before updating $\varrho(t; M_r) \rightarrow \varrho(t; M_r + 1)$. More specifically, an element of the density matrix, $\varrho_{ls}(t)$, should be sampled as

$$\varrho_{ls}(t; M_r) = \frac{1}{M_r} \sum_{j=1}^{M_r} c_{j,l}(t) \cdot c_{j,s}^\dagger(t), \quad (4)$$

where $c_{j,l}(t)$ is the l -th coefficient of the expansion (in the same basis $\{|k\rangle\}$, $k = 1, \dots, N$ used to express the density matrix) of the normalized wave-function, $|\psi_j(t)\rangle = \sum_{k=1}^N c_{j,k}(t) |k\rangle$.

The above recipe contains two key steps: (i) propagation (step 3) and (ii) determination of the time of the next jump (step 4). The waiting time, i.e., the time between two consecutive jumps, cannot be obtained without actual propagation of the trajectory (except in a few cases [38, 23]). This time must be obtained along with the numerical integration by using the non-Hermitian Hamiltonian $\tilde{H}(t)$. Practically, one has to propagate a trajectory, monitor the decaying squared norm of the wave vector and determine the instant of time when the squared norm equals η . In most of the existing studies, this was realized with a step-by-step Euler method. This approach, although having an independent physical interpretation [38], is not suitable for our purpose because it corresponds to the expansion of Eq. (1)

to the first order in time step δt ; consequently, a reasonable accuracy of the sampling can be achieved with extremely small values of δt only³.

Several improvements based on higher-order (with respect to δt) unraveling schemes [45, 46] have been put forward. The accuracy of the sampling – for the same number of realizations M_r and time step δt – can be improved substantially by increasing the order of the integration scheme [45]. In QuTiP, an open-source toolbox in Python to simulate dynamics of open quantum systems [35], Adams method (up to 12-th order) and backward differentiation formula (up to fifth order) with adaptive time step are implemented. To the best of our knowledge, this is presently the most accurate implementation⁴. In addition, QuTiP supports time-dependent Hamiltonians and allows for multi-processor parallelization.

In principle, QuTiP presents a suitable choice for our purpose. However, we are specially concerned about two issues. First there is the accuracy of propagation. As t_p has to be extremely large in order to be able to sample a state close to the attractor state ρ^{att} (note that up to now the method of quantum trajectories was used mainly to analyze short-time relaxation and transient regimes; e.g. see in Refs. [21, 22]), the accumulating error due to the discrete approximation of the continuous evolution with the effective Hamiltonian \tilde{H} can emerge sizable. These errors may induce serious problems, for example, when dealing with the delicate issue of MBL phenomena [47, 48].

Second, in the limit of weak dissipation when the coupling rates γ_k are small, jumps occur rarely. For most of the time the evolution of the trajectory is deterministic and a propagation using a small δt will not be efficient. Increasing the time step implies a decrease of the accuracy of determination of the time of the jump. This constitutes yet another factor which can blur the quality of the sampling scheme. If these two problems are successfully overcome, the only remaining problem left is to obtain a sufficiently large number of realizations. Here we handle both issues with an approach presenting an alternative to the schemes which rely on a method of increasing the order of integration.

A quantum trajectory serves a typical example of the so-called “event-driven processes” used in control theory [49] (where they are known as “Lebesgue sampling processes”) and computational neuroscience [50]. The question how to integrate such processes *numerically exact* is discussed in those latter research areas since the late 1990s. A possible option is the combination of exponential propagation together with time-stepping techniques. Here we follow the ideas presented in Ref. [50].

³A generalization of the TEBD technique to non-Hermitian operators was used for the propagation step in Refs. [43, 44]. Similar to its Hermitian predecessor [37], this method can only be used for lattice-like systems and guarantees correct asymptotic results only when there is no entanglement build-up in the course of the evolution.

⁴In the original publication [35], a model with $N = 8000$ states was probed. However, the issue was the performance of the program, so the computation time to propagate a single trajectory to a certain t_p was therein used as a quantifier.

First, consider a time-independent Hamiltonian $H(t) \equiv H$. The propagation over any time interval δt with the corresponding effective Hamiltonian \tilde{H} can be performed by the propagating operator (propagator) $P_{\delta t} = e^{-i\tilde{H}\delta t}$. Exponentiation of \tilde{H} can be performed numerically with controllable accuracy by implementing the scaling and squaring method [51]. To determine the time of the next jump, we use a time stepping technique [50]. We choose the convenient and efficient bisection method [52], cf. Section 5 for more details. The accuracy of the bisection method is controlled by the maximal order of bisections S which we call ‘maximal depth’. The time of the jump is thus resolved with a precision $2^{-S}\delta t$. A practical realization of this method demands a set of S propagators, that is, $P_{\delta t_s} = e^{-i\tilde{H}\delta t_s}$, $\delta t_s = 2^{-s}\delta t_0$, $s = 0, \dots, S$, that are complex $N \times N$ matrices. These propagators have to be pre-calculated and then stored. Generalization of this approach to the case of quench-like modulations is straightforward. In the bi-Hamiltonian case, see Eq. (2), we have to double the number of the stored propagators and then switch between the two sets every half of modulation period T . Note that we neither plan to outperform QuTiP with our algorithm nor to prove its superior accuracy. Our key objective here is to estimate the maximal size N_{max} of systems, Eqs. (1,2), whose asymptotic density matrix can be resolved with quantum trajectories on a supercomputer or on a computation cluster.

3. Statistical error(s) of sampling

We next briefly discuss the issue of statistical errors. Consider the sampling of a variable $X(t)$ over an ensemble of realizations $\{X_j(t)\}$, $j = 1, \dots, M_r$, with the aim to estimate its mean $\tilde{X}(t)$. Examples are the expectation value of an operator [39, 38, 40, 41] or an element of the density matrix (as in our case). In addition to the mean (average) of the variable, $\tilde{X}(t; M_r) = \frac{1}{M_r} \sum_{j=1}^{M_r} X_j(t)$, we can also calculate its variance [23, 41],

$$\text{var}[X(t); M_r] = \frac{1}{M_r} \sum_{j=1}^{M_r} (X_j(t) - \tilde{X}(t; M_r))^2, \quad (5)$$

which, for systems with a finite Hilbert space dimension N assumed here, converges to a generally time-dependent value $\text{var}[X(t)]$ in the limit $M_r \rightarrow \infty$. Different trajectories are statistical independent; therefore, the central limit theorem applies and, for large M_r , the probability density function (pdf) of the mean $\tilde{X}(t; M_r)$ can be approximated by a Gaussian pdf centered at $\tilde{X}(t)$ with the standard deviation $\sigma(t; M_r) = \sqrt{\text{var}(X; M_r)/M_r} \stackrel{M_r \gg 1}{\sim} M_r^{-\frac{1}{2}}$.

In the framework of local and global quantities [39], elements of the density matrix correspond to the former. In addition, they are small for large N , $\rho_{kl} \sim O(N^{-1})$, and the standard criterium of a trustful sampling, $\sigma(M_r)/\rho_{kl} \ll 1$, implies that $M_r \gg N^2$. Such a massive sampling is unfeasible if $N \gtrsim 10^3$, even when implemented on a supercomputer. However, this is a sufficient condition which (hopefully) greatly overestimates the number of realizations needed for a resolution of the density

matrix. This is another aspect of the sampling with quantum trajectories we like to obtain an insight.

Another relevant point is the time evolution of the variance $\text{var}[\rho_{kl}(t)]$. Evidently, it cannot grow to infinity simply because the absolute values of the coefficients $c_s(t)$, Eq. (4), do not exceed one. Therefore, there is an upper limit $\text{var}[\rho_{kl}(t)] \simeq 1$. On the other hand, for completely random and uniformly distributed values of $c_s(t)$ we find $\text{var}[\rho_{kl}(t)] \propto N^{-1}$. By using a scalable model we show that (i) the variances saturate in course of time to time-periodic values, $\text{var}[\rho_{kl}(t+T)] = \text{var}[\rho_{kl}(t)]$, which in addition (ii) allow for an accurate estimation of the density matrix elements using between $10^5 - 10^6$ realizations.

4. Model

As a testbed model we use a system of $N-1$ indistinguishable interacting bosons hopping between the sites of a periodically rocked dimer. The system Hamiltonian reads

$$H(t) = -J(b_1^\dagger b_2 + b_2^\dagger b_1) + \frac{U}{2(N-1)} \sum_{g=1,2} n_g (n_g - 1) + \varepsilon(t) (n_2 - n_1). \quad (6)$$

Here, J denotes the tunneling amplitude, U is the interaction strength, and $\varepsilon(t)$ presents a periodically temporal modulation of the local potential. In particular, we choose $\varepsilon(t) = \varepsilon(t+T) = \mu_0 + \mu_1 Q(t)$, where μ_0 and μ_1 are a static and a dynamically varying energy offset between the two sites, respectively. $Q(t)$ denotes a periodically varying, two-valued quench within one full period T , i.e., $Q(\tau) = \frac{1}{2}$ within $0 < \tau \leq T/2$ and $Q(\tau) = -\frac{1}{2}$ for the second half period $T/2 < \tau \leq T$. The boson operators b_g and b_g^\dagger are the annihilation and creation operators on site $g \in \{1, 2\}$, while $n_g = b_g^\dagger b_g$ is the particle number operator. The system Hilbert space has dimension N and can be spanned with the N Fock basis vectors, labeled by the number of boson on the first site n , $\{|n+1\rangle\}$, $n = 0, \dots, N-1$. Thus, the model size is controlled by the total number of bosons. Hamiltonian (6) has been used for theoretical studies [53, 54, 55] and was implemented in experiments [56, 57].

We use a single jump operator [58, 59],

$$V = (b_1^\dagger + b_2^\dagger)(b_1 - b_2), \quad (7)$$

which ‘synchronizes’ the dynamics on the sites by constantly recycling anti-symmetric out-phase mode into symmetric in-phase one. The dissipative coupling constant $\gamma = \gamma_0/(N-1)$ is assumed to be time-independent. Since the jump operator is non-Hermitian, the propagators \mathcal{P}_t are not unital and the attractor does not assume the maximally mixed state, $\rho^{\text{att}} \neq \mathbb{1}/N$.

The Hamiltonian (6) is non-integrable when $U \neq 0$; therefore, an analytical solution of the corresponding Lindblad equation is not known. However, in the limit $N \rightarrow \infty$ the dynamics can be approximated by mean-field equations for the expectation values of the three pseudo-spin operators $S_x = \frac{1}{2(N-1)}(b_1^\dagger b_2 + b_2^\dagger b_1)$, $S_y = -\frac{i}{2(N-1)}(b_1^\dagger b_2 - b_2^\dagger b_1)$, $S_z =$

$\frac{1}{2(N-1)}(n_1 - n_2)$. For a large number of atoms, the commutator $[S_x, S_y] = \frac{iS_z}{N-1} \stackrel{N \rightarrow \infty}{\approx} 0$ and similarly for other cyclic permutations. Replacing operators with their expectation values, $\langle S_k \rangle = \text{tr}[\rho S_k]$, and denoting $\langle S_k \rangle$ by S_k , we find the semi-classical equations of motion [60]

$$\begin{aligned} \frac{dS_x}{dt} &= 2\varepsilon(t)S_y - 2US_zS_y + 8\gamma_0(S_y^2 + S_z^2), \\ \frac{dS_y}{dt} &= -2\varepsilon(t)S_x + 2US_xS_z + 2JS_z - 8\gamma_0S_xS_y, \\ \frac{dS_z}{dt} &= -2JS_y - 8\gamma_0S_xS_z. \end{aligned} \quad (8)$$

As $S^2 = S_x^2 + S_y^2 + S_z^2 = 1/4$ is a constant of motion, we can reduce the mean-field evolution to the surface of a Bloch sphere, $(S_x, S_y, S_z) = \frac{1}{2}[\cos(\varphi)\sin(\vartheta), \sin(\varphi)\sin(\vartheta), \cos(\vartheta)]$, yielding the equations of motion

$$\begin{aligned} \dot{\varphi} &= 2J \frac{\cos(\vartheta)}{\sin(\vartheta)} \cos(\varphi) - 2\varepsilon(t) + U \cos(\vartheta) - 4\gamma_0 \frac{\sin(\varphi)}{\sin(\vartheta)}, \\ \dot{\vartheta} &= 2J \sin(\varphi) + 4\gamma_0 \cos(\varphi) \cos(\vartheta). \end{aligned} \quad (9)$$

The density matrix ρ of the system with $N-1$ bosons can be visualized on the same Bloch sphere by plotting the Husimi distribution $p(\vartheta, \varphi)$, obtained by projecting ρ on the set of the generalized SU(2) coherent states, $|\theta, \varphi\rangle = \sum_{j=0}^{N-1} \sqrt{\binom{N-1}{j}} [\cos(\theta/2)]^j [e^{i\varphi} \sin(\theta/2)]^{N-1-j} |j\rangle$ [61, 62]. Visual comparison of the Husimi distribution with the mean-field solution, Eq. (9), will serve as a simple test of the meaningfulness of the sampled density matrix $\rho(t_p; M_T)$.

5. Implementation on a supercomputer and performance

Here we describe a high-performance implementation of the algorithm on a supercomputer and analyze its scalability by using the model system (6, 7). Numerical experiments were performed on the ‘‘Lobachevsky’’ supercomputer at the Lobachevsky State University of Nizhny Novgorod [63]. We employed up to 32 computing nodes, with the following configuration per node: 2× Intel Xeon E5-2660 CPU (8 cores, 2.2 GHz), 64 GB RAM, OS CentOS 6.4. We use Intel Math Kernel Library (MKL), Intel C/C++ Compiler, and Intel MPI from Intel Parallel Studio XE [64].

Following Eq. (3), we start with two effective non-Hermitian Hamiltonians, \tilde{H}_1 and \tilde{H}_2 , describing the quench-like modulations, Eq. (2), as represented by a pair of complex double-precision $N \times N$ matrices. An initial pure state $|\psi^{\text{init}}\rangle$ is represented by a complex-valued double-precision vector. The propagation operator yields a wave function for a single sample. We follow the straightforward approach to parallelization with an independent random sampling. Namely, the computational load is distributed among supercomputer nodes by the standard Message Passing Interface (MPI). On each node we employ the OpenMP threads to parallelize sampling. Computationally intensive operations are implemented by calling BLAS functions from Intel MKL in sequential mode.

Algorithm 1 : propagation of a quantum trajectory with exponential operators and bisection method

```
1: set  $\delta t = \delta t_0$  &  $s = 0$ 
2: while  $\|\psi(t)\|^2 > \eta$  do
3:   calculate  $|\tilde{\psi}(t)\rangle = P_{\delta t}|\psi(t)\rangle$ 
4:   if  $\|\psi(t)\|^2 < \eta$  &  $s < S$  then
5:      $s = s + 1$ 
6:   else
7:      $|\psi(t)\rangle = |\tilde{\psi}(t)\rangle$ 
8:      $t = t + \delta t$ 
9:     while  $s > 0$  &  $\delta t = n \cdot \delta t_{s-1}, n \in \mathbb{Z}^+$  do
10:       $s = s - 1; \delta t = \delta t_s$ 
11:     end while
12:   end if
13: end while
```

The code consists of three main steps. First, the program initializes MPI, allocates memory, reads parameters and the matrices of the pre-calculated exponential propagators from configuration files. The propagators are calculated independently on each cluster node. In a second step all OpenMP threads in all MPI processes independently propagate several quantum trajectories starting from the initial state $|\psi^{\text{init}}\rangle$. The propagation is realized with the step-decimation technique described in Section 2. The pseudo-code is presented in Algorithm 1. The maximal depth S , the time steps $\delta t_s = 2^{-s} dt$, and the exponential propagators $P_{\delta t_s}$, $s = 0, \dots, S$ are pre-loaded. The program is initiated with $s = 0$, but later s is taken from the previous propagation loop step. This step is fully parallel; it contains a matrix-vector multiplication that is the most computationally intensive part of the algorithm. This operation is performed with the `zgemv` MKL subroutine. During the third step all samples on each node are accumulated into the density matrix. Next, these matrices are collected in the rank 0 MPI process. Finally, one evaluates the resulting density matrix. This matrix is written to the output file, the dynamic memory is deallocated and the MPI is finalized.

The efficient utilization of a supercomputer requires a reasonable scaling on the distributed memory. In this regard, quantum trajectories possess an ideal parallelization potential. The method realizes the general Monte Carlo paradigm with independent simulations and without substantial load imbalance. The transfer of the resulting data is the only data interchange between nodes. We ran numerical simulations utilizing up to 32 nodes of the supercomputer and found that the implementation scales almost linearly with the number of nodes. Next, we

Table 1: Scaling efficiency on shared memory.

Number of threads	Time of computations, in seconds	Efficiency, percent
1	2170	100
2	1114	97
4	557	97
8	292	93
16	156	87

consider the performance and the scaling efficiency of the implementation on 16 CPU cores with shared memory. To start, the number of MPI processes and OpenMP threads have to be chosen. We tried several different configurations; namely, 1 process \times 16 threads, 2 processes \times 8 threads, 4 processes \times 4 threads, 8 processes \times 2 threads, and 16 processes \times 1 thread. We did not find a substantial difference in performance and chose the option 1 MPI process with 16 OpenMP threads mode for simulations. It is known that setting a relevant affinity mask to pin threads to CPU cores usually affects performance and scalability. In this regard, we used the following settings: `KMP_AFFINITY=granularity=fine,scatter`. For all performance measurements in this section we considered the model setup, Eqs. (6, 7), with 63 bosons (i.e., with dimension $N = 2^6 = 64$) and 640 trajectories. The results of our computational experiments are summarized in Table 1. Upon inspection this shows that our implementation allows 87% scaling efficiency on 16 CPU cores with shared memory.

Then we ran the Intel VTune Amplifier XE profiler to find main time-consuming parts of our implementation. As a result we found that the high-performance implementation of the dense matrix-vector multiplication with `zgemv` takes more than 99% of the total computation time. This in turn means that there is no potential for further optimization of the code.

Table 2: Single-core computation time to propagate a trajectory over one period T as a function of N . The parameters are $J = 1$, $\mu_0 = 1.5$, $\mu_1 = 1$, $U = 3$, $\gamma_0 = 0.1$, and $S = 20$.

Number of states, N	Time of computations, in seconds
64	0.37
128	2.3
256	16
512	153
1024	1153
2048	8642
4096*	64785

* extrapolation

Finally, we estimated the computation time to propagate a single trajectory on a single-core as a function of system size

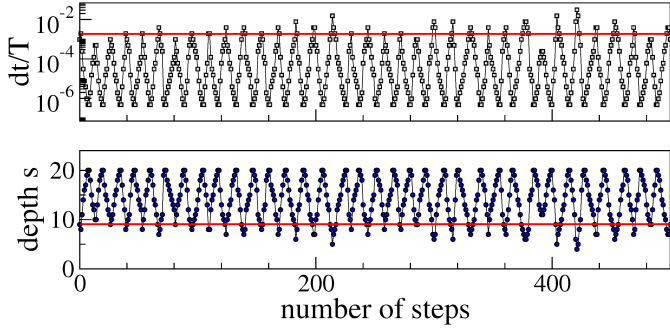


Figure 2: (color online) Float-like performance of Algorithm 1 during the propagation of a quantum trajectory. Every local maximum in the dependence dt vs number of steps (minimum in the depth s dependence) indicates an occurrence of a jump after which the algorithm performs a chain of bisections to reach the maximal depth $S = 20$. After every step during which no jump occurred, the algorithm doubles the step size. The average time between two consecutive jumps (red line) is the average height of the local maximum minus 1 (this is because of the first step needed to recognize the jump appearance). The two sequences were monitored during the sampling of the asymptotic state.

N , see Table 2. For the model specified by Eqs. (6, 7) this time scales as N^3 ; this is due to the multiplication of the quadratic scaling of a dense matrix-vector multiplication and a linear scaling of the jump frequency. The latter scaling is, however, model specific and may differ for other physical systems so that the overall computation time may vary substantially with the type of Hamiltonian and/or dissipators under study. On top, the numbers we present in Table 1 depend on the values of the coupling constant γ_0 and the period of modulations T . This is so because these parameters control the rate of the jumps. Therefore, the obtained estimates are specific and cannot be used as universal quantifiers.

6. Applications

We now report the results of our simulations obtained for the physical setup with Eqs. (6, 7). We start with the performance of the algorithm, Table 1. The idea of the algorithm mimics a float: The algorithm constantly attempts to ‘float to the surface’, i.e., to increase the time step of integration towards its maximal value δt_0 while every next jump pulls it downwards to δt_S , see Fig. 2. The average time between two consequent jumps is the mean of the local maxima in the depicted saw-like time sequence of δt . There is no problem in overestimating δt_0 , simply because the time step will rarely reach its maximum. The shortest time step, δt_S , or, equivalently, the depth S , is tuned to the values needed to reach the desired accuracy.

Next we turn to the averages $\bar{\varrho}_{kl}^{\text{att}}(t)$ over the realizations and the corresponding statistical variances $\text{var}[\varrho_{kl}^{\text{att}}(t)]$ of the matrix elements, as discussed in detail in Section 3. Both quantities converge to “limit cycles” if the propagation time $t_p = nT + \tau$, $n \in \mathbb{Z}^+$, $\tau \in [0, T)$, is much larger than all relaxation times. This means that for $n \gg 1$ the density matrix converges to a time-periodic quantum attractor, i.e., $\bar{\varrho}(nT + \tau) \simeq \bar{\varrho}^{\text{att}}(\tau)$, and the variances also become time-periodic functions, $\text{var}[\varrho_{kl}(nT + \tau)] \simeq \text{var}[\varrho_{kl}^{\text{att}}(\tau)]$, see Fig. 3b. The crumpled caustic-like shapes of the

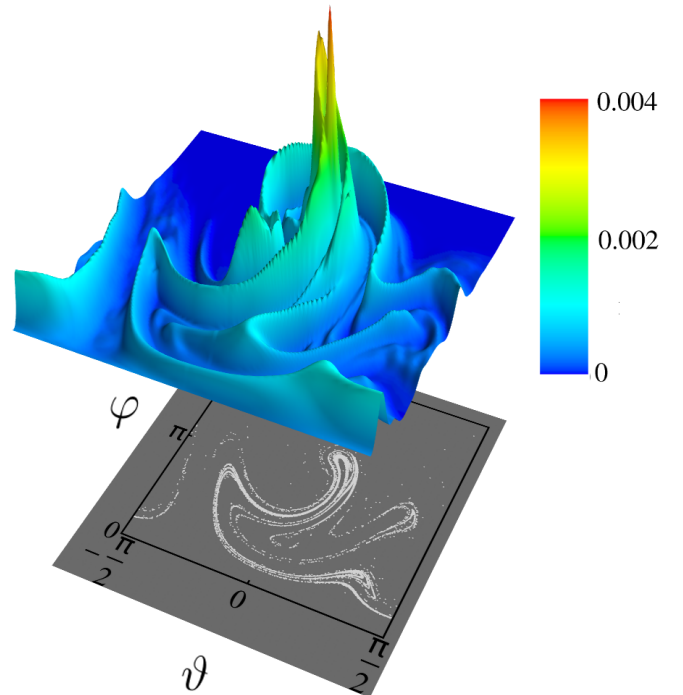


Figure 4: Attractors of the dimer model, Eqs. (6, 7). Husimi distribution of the attractor density matrix $\varrho^{\text{att}}(0)$ of the dimer with $N - 1 = 1023$ bosons (top) and classical attractor of the mean-field systems, Eq. (9) (bottom panel). The density matrix was sampled with 10^5 stroboscopic realizations. The parameters are $J = 1$, $\mu_0 = 1.5$, $\mu_1 = 1$, $U = 3$, $\gamma_0 = 0.1$.

limit cycles is a result of the projection on a plane of a global limit-cycle living in N^4 -dimensional space. This limit-cycle is not a topological product of N^2 two-dimensional limit cycles; elements of the asymptotic density matrix do not evolve independently, they do interact so that their means and variances are coupled.

In the asymptotic regime sampling can be performed stroboscopically, i.e., after every period T . In our simulations we used as the transient time $t_p = 1000T$ and then performed the stroboscopic sampling of $\varrho^{\text{att}}(\tau = 0)$. The attractor density matrix at any other instant of time τ can be sampled by shifting the starting time of the sampling, $t_p \rightarrow t_p + \tau$, or simply by performing an extra-sampling at all needed intermediate points.

With 4000 samples per trajectory (that amounts to an additional propagation for the time $4000T$) it became possible to collect $M_T = 10^5$ samples for the model of dimension $N = 1024$ (i.e., with $N - 1 = 1023$ indistinguishable bosons) by running the program on 32 cores during three days. For some choice of parameters the sample density matrix displays a standard diagonal-dominated structure, see Fig. 3a. The Husimi distribution of the sample density matrix is depicted in Fig. 4. There is an intriguing similarity between the distribution of the quantum attractor and the phase-space structure of the classical attractor (its stroboscopic section, to be more precise) produced by the mean-field equations, Eqs. (9). This allows us to conjecture that the attractor density matrix is resolved with good accuracy. The 128 cores allowed us to sample the same number of realizations for the model of the dimension $N = 2048$ during approximately one week⁵.

7. Summary and Outlook

The primary aim of this study was to estimate the numerical horizon of a high-accuracy sampling of non-equilibrium dissipative quantum attractors, i.e., the asymptotic solutions of periodically driven open systems, by using the quantum trajectory method. Our main result is that it is possible to resolve asymptotic density matrices of systems of several thousand of states by using even a small cluster (with ≥ 128 cores) on a time scale of a few days. The benefit of having access to the whole density matrix is the possibility to extract more detailed information about non-equilibrium regimes encoded in the matrix structure such as purity and many-body entanglement [65].

Naturally, the next step must be a systematic analysis of the errors, statistical and numerical ones. We reserve this objective for further studies. Here, we would like to surmise on further optimization of the sampling procedure. An immediate idea is to use a reduced adaptive basis, constructed by using coherent states [66]. This however demands a priori knowledge of the attractor's structure. This insight can be obtained by using models of small sizes, $N \sim 10^2$. Another possibility is the

choice of more optimal initial conditions which in turn will substantially reduce the transient time t_p (for example, one can use an extrapolation of the largest-eigenvalue eigenstate of the density matrix for a small system). Altogether, we expect that such improvements could increase N further by a factor of $\sim 2 - 3$.

Research areas where quantum attractors are of potential interest were already mentioned in Section 1. Here, we briefly recall them. First, this is many-body localization [17] where the action of temporal modulations [18, 19] and dissipation [20, 21] so far have been considered separately. A combined action of both factors presents an intriguing challenge. A complementary task is to extend the idea of “dissipative engineering” [1, 2, 3] to periodically-modulated quantum systems. Finally, a survival of Floquet topological insulators [14] in the presence of dissipation is a timely question.

8. Acknowledgments

The authors acknowledge support by the Russian Science Foundation (grant No. 15-12-20029). We thank I. Vakulchik for the help with preparing the figures.

References

- [1] B. Kraus *et al.*, Phys. Rev. A **78** (2008) 042307.
- [2] J. T. Barreiro *et al.*, Nature Phys. **6** (2010) 943.
- [3] D. Kienzler *et al.*, Science **347** (2015) 53.
- [4] F. Pastawski, L. Clemente, and J. I. Cirac, Phys. Rev. A **83** (2011) 012304; M. J. Kastoryano, M. M. Wolf, and J. Eisert, Phys. Rev. Lett. **110** (2013) 110501; E. Kapit, Phys. Rev. Lett. **116** (2016) 150501.
- [5] J. H. Shirley, Phys. Rev. **138** (1965) B979.
- [6] H. Sambe, Phys. Rev. A **7** (1973) 2203.
- [7] M. Grifoni and P. Hänggi, Phys. Rep. **304** (1998) 229.
- [8] A. Eckardt and E. Anisimovas, New J. of Phys. **17** (2015) 093039.
- [9] S. Kohler, J. Lehmann and P. Hänggi, Phys. Rep. **406** (2005) 379.
- [10] E. Arimondo, D. Ciampini, A. Eckardt, M. Holthaus, and O. Morsch, Adv. At. Mol. Opt. Phys. **61** (2012) 515.
- [11] M. Bukov, L. D’Alessio, and A. Polkovnikov, Adv. Phys. **64** (2015) 139.
- [12] A. Eckardt, *Atomic quantum gases in periodically driven optical lattices*, arXiv:1606.08041.
- [13] J. Gong, L. Morales-Molina, and P. Hänggi, Phys. Rev. Lett. **103** (2009) 133002.
- [14] N. H. Lindner, G. Refael, and V. Galitski, Nature Phys. **7** (2011) 490.
- [15] D. E. Liu, A. Levchenko, and H. U. Baranger, Phys. Rev. Lett. **111** (2013) 047002; A. Kundu and B. Seradjeh, Phys. Rev. Lett. **111** (2013) 136402.
- [16] N. Goldman and J. Dalibard, Phys. Rev. X **4** (2014) 031027.
- [17] D. M. Basko, I. L. Aleiner, and B. L. Altshuler, Ann. Phys. **321** (2006) 1126;
- [18] P. Ponte, Z. Papić, F. Huveneers, and D. Abanin, Phys. Rev. Lett. **114** (2015) 140401.
- [19] A. Lazarides, A. Das, and R. Moessner, Phys. Rev. Lett. **115** (2015) 030402.
- [20] M. F. Fisher, M. Maksymenko, E. Altman, Phys. Rev. Lett. **116** (2016) 160401.
- [21] E. Levi, M. Heyl, I. Lesanovsky, J. P. Garrahan, Phys. Rev. Lett. **116** (2016) 237203.
- [22] B. Everest, I. Lesanovsky, J. P. Garrahan, E. Levi, *Role of interactions in a dissipative many-body localized system*, arXiv:1605.07019 (2016).
- [23] Breuer, H.-P., and F. Petruccione, *The Theory of Open Quantum Systems* (Oxford University Press, Oxford, 2002).
- [24] H.J. Carmichael, *An Open Systems Approach to Quantum Optics* (Springer, Berlin, 1993).
- [25] G. Lindblad, Commun. Math. Phys. **48** (1976) 119.
- [26] Alicki, R., and K. Lendi, 1987, *Quantum Dynamical Semigroups and Applications*, Lecture Notes in Physics, vol. 286 (Springer, Berlin, 1998).

⁵Calculations of the Husimi distribution for the model (6, 7) involve summation over series of binomial coefficients of the order N . It was not possible, however, to go beyond $N = 2^{10} = 1024$ when evaluating the corresponding Husimi distributions.

- [27] K. Kraus, *States, effects and operations: fundamental notions of quantum theory*, Lecture Notes in Physics, vol. 190 (Springer, Berlin, 1983).
- [28] H. Spohn, Rep. Math. Phys. **10** (1976) 198.
- [29] B. Baumgartner and H. Narnhofer, J. Phys. A: Math. and Theor. **41** (2008) 395303.
- [30] K. Lendi, Phys. Rev. A **33** (1986) 3358.
- [31] A. Lazarides, A. Das, and R. Moessner, Phys. Rev. E **90** (2014) 012110.
- [32] L. D'Alessio and M. Rigol, Phys. Rev. X **4** (2014) 041048.
- [33] V. A. Yakubovich and V. M. Starzhinski, *Linear Differential Equations with Periodic Coefficients* (John Wiley & Sons, New York, 1975).
- [34] P. D. Nation, J. R. Johansson, M. P. Blencowe, and A. J. Rimberg, Phys. Rev. E **91** (2015) 013307.
- [35] R. Johansson, P.D. Nation, F. Nori, Comp. Phys. Comm. **183** (2012) 1760
- [36] W. Huisinga, L. Pesce, R. Kosloff, and P. Saalfrank, J. Chem. Phys. **110** (1999) 5538.
- [37] M. Zwolak and G. Vidal, Phys. Rev. Lett. **93** (2004) 207205.
- [38] R. Dum, A.S. Parkins, P. Zoller, and C.W. Gardiner, Phys. Rev. A **46** (1992) 4382.
- [39] K. Mølmer, Y. Castin, and J. Dalibard, J. Opt. Soc. Am. B **10** (1993) 524.
- [40] M. B. Plenio and P. L. Knight, Rev. Mod. Phys. **70** (1998) 101.
- [41] A. J. Daley, Adv. Phys. **63** (2014) 77.
- [42] I. Foster, *Designing and Building Parallel Programs* (AddisonWesley, 1995).
- [43] A. J. Daley, J. M. Taylor, S. Diehl, M. Baranov, P. Zoller, Phys. Rev. Lett. **102** (2009) 040402.
- [44] L. Bonnes and A.M. Läuchli, *Superoperators vs. trajectories for matrix product state simulations of open quantum system: a case study*, arXiv:1411.4831.
- [45] J. Steinbach, B. M. Garraway, and P. L. Knight, Phys. Rev. A **51** (1995) 3302.
- [46] H.-P. Breuer, U. Dorner, F. Petruccione, Comp. Phys. Comm. **132** (2000) 30.
- [47] D. J. Luitz, N. Laflorencie, and F. Alet, Phys. Rev. B **91**, 081103 (2015); M. Serbyn, Z. Papic, and D. A. Abanin, Phys. Rev. X **5** (2015) 041047.
- [48] W. de Roeck, F. Huveneers, M. Müller, and M. Schiulaz, Phys. Rev. B **93** (2016) 014203.
- [49] K. J. Åström and B. Bernhardsson, *Comparison of periodic and event based sampling for first-order stochastic systems*. In Preprints 14th World Congress of IFAC, Beijing, P.R. China, July 1999.; K. J. Åström and B. Bernhardsson, Lecture Notes in Control and Information Sciences **286** (2002) 1.
- [50] S. Rotter and M. Diesmann, Biol. Cybern. **81** (1999) 381.
- [51] C. Moler and Ch. Van Loan, SIAM Rev. **45** (2003) 3.
- [52] D. E. Knuth, *The art of computer programming*, v. 3 (Pearson Ed., US, 1998).
- [53] A. Vardi, J. R. Anglin, Phys. Rev. Lett. **86** (2001) 568.
- [54] F. Trimborn, D. Witthaut, S. Wimberger, J. Phys. B: At. Mol. Opt. Phys. **41** (2008) 171001.
- [55] D. Poletti, J.-S. Bernier, A. Georges, C. Kollath, Phys. Rev. Lett. **109** (2012) 045302.
- [56] C. Gross, T. Zibold, E. Nicklas, J. Esteve, M.K. Oberthaler, Nature **464** (2010) 1165.
- [57] J. Tomkovič, W. Muessel, H. Strobel, S. Löck, P. Schlagheck, R. Ketzerick, M. K. Oberthaler, *Observing the emergence of chaos in a many-particle quantum system*, arXiv:1509.01809.
- [58] S. Diehl, A. Micheli, A. Kantian, B. Kraus, H. P. Büchler, P. Zoller, Nature Physics **4** (2008) 878.
- [59] S. Diehl, A. Tomadin, A. Micheli, R. Fazio, P. Zoller, Phys. Rev. Lett. **105** (2010) 015702.
- [60] M. Hartmann, D. Poletti, M. Ivanchenko, S. Denisov, P. Hänggi, *Asymptotic state of many-body open quantum systems under time-periodic modulations*, arXiv:1606.03896.
- [61] F. T. Arecchi, E. Courtens, R. Gilmore, and H. Thomas, Phys. Rev. A **6** (1972) 2211.
- [62] A. Perelomov, *Generalized Coherent States and their Applications* (Springer, Berlin 1986).
- [63] <http://www.top500.org/system/178472>
- [64] Intel® Parallel Studio XE 2015. <https://software.intel.com/en-us/intel-parallel-studio-xe>
- [65] F. Benatti, R. Floreanini, U. Marzolino, Ann. Phys. **327** (2012) 1304.
- [66] T. Steimle, G. Alber and I. C. Percival, J. of Phys. A: Math. and Gen. **28** (1995) L491;

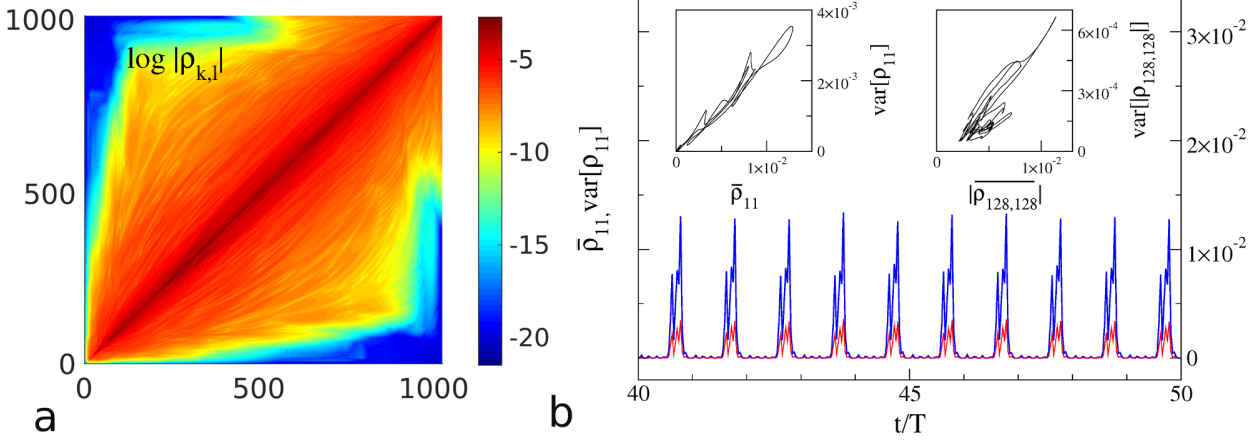


Figure 3: (a) Structure of the sampled stroboscopic density matrix $\varrho^{\text{att}}(0)$ ($N = 1024$) and (b) time evolution of the mean $\bar{\varrho}_{11}(t)$ (thick blue line) and variance $\text{var}[\varrho_{11}(t)]$ (thin red line) for $t \in [40T, 50T]$ ($N = 256$). In both cases the sampling was performed over 10^5 independent trajectories initiated at the state $|\psi^{\text{init}}\rangle = |1\rangle$. The inset depicts the limit-cycle evolution of the means and variances for two diagonal elements, $\varrho_{1,1}$ and $\varrho_{128,128}$, during one period of modulations, $t \in [1000T, 1001T]$. Curves for latter periods are indistinguishable from the presented ones. The parameters are the same as in Fig. 2.